

NDB  
IN-16-TM  
009 133

# **Experimental and Computational Analysis of Shuttle Orbiter Hypersonic Trim Anomaly**

Gregory J. Brauckmann, John W. Paulson Jr.,  
K. James Weilmuenster

Reprinted from

## **Journal of Spacecraft and Rockets**

Volume 32, Number 5, Pages 758-764



*A publication of the*  
American Institute of Aeronautics and Astronautics, Inc.  
370 L'Enfant Promenade, SW  
Washington, DC 20024-2518

# Experimental and Computational Analysis of Shuttle Orbiter Hypersonic Trim Anomaly

Gregory J. Brauckmann,\* John W. Paulson Jr.,† and K. James Weilmuenster‡  
 NASA Langley Research Center, Hampton, Virginia 23681-0001

**During the high-Mach-number, high-altitude portion of the first entry of the Shuttle Orbiter, the vehicle exhibited a nose-up pitching moment relative to preflight prediction of approximately  $\Delta C_m = 0.03$ . This trim anomaly has been postulated to be due to compressibility, viscous, and/or real-gas (lowered specific heat ratio  $\gamma$ ) effects on basic body pitching moment, body-flap effectiveness, or both. In order to assess the relative contribution of each of these effects, an experimental study was undertaken to examine the effects of Mach number, Reynolds number, and ratio of specific heats. Complementary computational solutions were obtained for wind-tunnel and flight conditions. The primary cause of the anomaly was determined to be lower pressures on the aft windward surface of the Orbiter than deduced from hypersonic wind-tunnel tests with ideal- or near-ideal-gas test flow. The lower pressure levels are a result of the lowering of the flowfield  $\gamma$  due to high-temperature effects. This phenomenon was accurately simulated in a hypersonic wind tunnel using a heavy gas, which provided a lower  $\gamma$ , and was correctly predicted by Navier–Stokes computations using nonequilibrium chemistry.**

## Nomenclature

$b$	= reference wingspan, in.
$C_m$	= pitching-moment coefficient, pitching moment / $q_\infty S c$
$C_N$	= normal-force coefficient, normal force / $q_\infty S$
$C'$	= Chapman–Rubesin constant evaluated at reference temperature
$c$	= reference mean aerodynamic chord, in.
$e$	= static energy
$h$	= static enthalpy
$L$	= Shuttle Orbiter reference length, in.
$M_\infty$	= freestream Mach number
$P_t$	= stagnation pressure, psia
$P_{t2}$	= pitot pressure, psia
$Re_\infty$	= freestream unit Reynolds number, $\text{ft}^{-1}$
$Re_{\infty,L}$	= Reynolds number based on reference length
$S$	= reference area, $\text{ft}^2$
$T_t$	= stagnation temperature, °R
$V_\infty$	= viscous-interaction parameter, $M_\infty \sqrt{(C') / \sqrt{(Re_{\infty,L})}}$
$\alpha$	= angle of attack, deg
$\gamma$	= ratio of specific heats, $h/e$
$\gamma_\infty$	= freestream specific heat ratio

## Introduction

**D**URING the high-Mach-number, high-altitude segment of the first entry of the Space Shuttle Orbiter, with laminar, continuum flow over the windward surface, the vehicle exhibited a nose-up pitching-moment increment ( $\Delta C_m$ ) relative to preflight prediction of approximately 0.03. This caused the body flap to deflect twice the amount thought necessary to achieve trimmed flight. This so-called pitch-up anomaly has been investigated<sup>1–4</sup> over the years, with explanations ranging from compressibility, to viscous, to real-gas (high-temperature) effects<sup>5</sup> on basic-body pitching moment and/or body-flap effectiveness. Compressibility and viscous effects, while affecting basic aerodynamics, also govern the behavior of flow separation ahead of deflected control surfaces. Low values of the Reynolds number, such as occur in flight at high

altitudes, may cause the flap to lose effectiveness by submerging it in a thick boundary layer such that the flap does not encounter the inviscid flow. In addition, high viscous shear of the crossflow in the nose region has been postulated as the mechanism to induce nose-up pitching moments.<sup>6</sup> High-temperature effects occur when air heats as it crosses the strong bow shock of the vehicle in hypersonic flight. The main consequences as far as aerodynamics are concerned are an increase in the shock density ratio, hence a decrease in the shock detachment distance and an alteration of the inviscid flowfield, and a lowering of the flowfield specific heat ratio.

Predicted aerodynamic characteristics of the Orbiter are documented in the preflight Aerodynamic Design Data Book (ADDB).<sup>7</sup> The data in this document span the Mach-number range from subsonic to hypersonic, and are a compilation of many hours of wind-tunnel testing. An advisory group was formed to analyze this large volume of data and to provide a best estimate of the flight aerodynamics.<sup>8</sup> This group decided the primary scaling parameter should be the length Reynolds number below a freestream Mach number of 15, and the viscous-interaction parameter  $V_\infty$  for flight above  $M_\infty = 15$ . Real-gas effects were considered<sup>9</sup> prior to flight, but uncertainties associated with the available data resulted in an adjustment to the tolerances (allowed error in prediction) rather than to the preflight estimates themselves.

In order to clarify and substantiate the causes of the flight-to-preflight discrepancies, a systematic study was undertaken to examine the effects of Mach number, Reynolds number, and real-gas effects on basic body pitching moment and body-flap effectiveness. Two approaches were used. First, conventional hypersonic wind tunnels, all with instrumentation upgrades and most with new nozzles that provide better flow uniformity, were used to examine the effects of Mach number and Reynolds number on configuration aerodynamics and control effectiveness. Effects due to specific heat ratio were examined in the 20-in. Mach 6  $\text{CF}_4$  tunnel, where testing in a heavy gas simulates the higher flight density ratio and lower specific heat ratio characteristic of a real gas. Second, a full Navier–Stokes computer code utilizing finite-rate chemistry was used to predict the flowfield over the entire orbiter windward geometry, including the deflected body flap, for both wind-tunnel and flight conditions. Comparisons are made between the present experimental results, computational predictions, the preflight aerodynamic data book released in 1980,<sup>7</sup> and aerodynamic coefficients derived from the flight of STS-1. The results of this study are expected to help define the optimum approach for the design of the next-generation space transportation system.

Received Feb. 3, 1994; revision received April 12, 1995; accepted for publication April 18, 1995. Copyright © 1995 by the American Institute of Aeronautics and Astronautics, Inc. No copyright is asserted in the United States under Title 17, U.S. Code. The U.S. Government has a royalty-free license to exercise all rights under the copyright claimed herein for Governmental purposes. All other rights are reserved by the copyright owner.

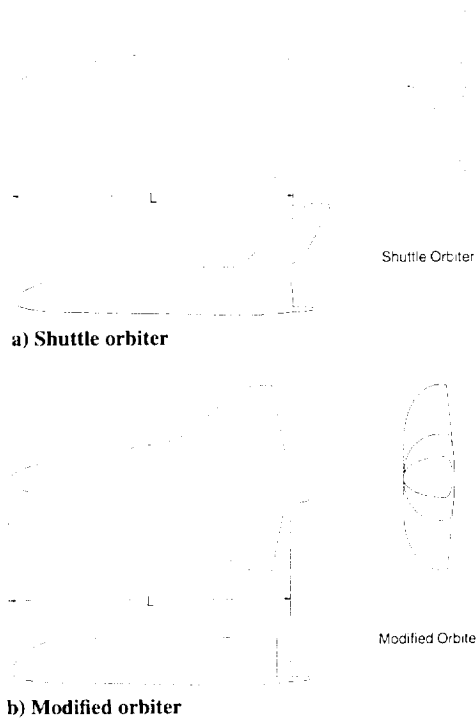
\*Research Engineer, Senior Member AIAA.

†Assistant Head, Aerothermodynamics Branch, Associate Fellow AIAA.

‡Senior Research Engineer, Associate Fellow AIAA.

**Table 1** Reference dimensions for various models

Model	Scale	$S_{ref}$ , ft <sup>2</sup>	$b$ , in.	$c$ , in.	$X_{c.g.}$ , in.	$Z_{c.g.}$ , in.	$L$ , in.
Shuttle	Full	2690.0	936.68	474.81	838.7	-25.0	1290.3
Shuttle	0.0040	0.0433	3.756	1.904	3.363	-0.100	5.174
Shuttle	0.0075	0.1513	7.025	3.561	6.290	-0.1875	9.677
Modified	0.0075	0.1513	7.025	3.561	6.290	-0.1875	9.677

**Fig. 1** Sketch of configurations used in this study.

## Experimental Method

### Models

Three models were used for this study. Two were scale models of the full Shuttle Orbiter configuration, with scales of 0.004 and 0.0075. Body-flap deflections tested were 0.0, 12.5, and 16.3 deg for the smaller model and 0.0, 16.0, and 20.0 deg for the larger model. The third model was a 0.0075-scale modified Orbiter geometry, which accurately represented the windward surface, including the body flap, but used elliptical cross sections to create the upper surface. All models were numerically machined from stainless steel. A verification check of the aerolines was performed prior to testing, and both larger models represented the shuttle windward surface aerolines within  $\pm 0.003$  in. The smaller model met this tolerance in general, but had deviations up to 0.008 in. along the windward centerline just behind the nose region (from 2 to 25% of the reference body length). A sketch of the geometries and reference dimensions are given in Fig. 1 and Table 1, respectively.

### Facilities

Five blowdown hypersonic wind tunnels were used in this study. They were the 15-in. Mach 6 Hi-Temperature Air Tunnel, 20-in. Mach 6 Tunnel, 31-in. Mach 10 Tunnel, 22-in. Mach 20 Helium Tunnel, and the 20-in. Mach 6 CF<sub>4</sub> Tunnel. The major components of each facility are a high-pressure bottlefield, settling chamber, nozzle, test section, diffuser, and vacuum spheres. The flow is heated by an electrical resistance heater in all facilities except the 22-in. Mach 20 Helium Tunnel and the 20-in. Mach 6 CF<sub>4</sub> Tunnel. The helium facility has the capability to heat the flow, but it is not needed to avoid flow liquefaction, and the CF<sub>4</sub> facility uses a lead bath heater. The helium and CF<sub>4</sub> facilities reclaim the test gas from the vacuum spheres; the others vent to atmosphere after the run is over. More detailed descriptions, and recent calibrations for several, are found in a paper by Miller.<sup>10</sup>

**Table 2** Nominal test conditions

Tunnel	Mach no.	Scale	$Re_{\infty}$ , 10 <sup>6</sup> ft <sup>-1</sup>	$Re_{\infty,L}$ , 10 <sup>6</sup>	$\gamma_{\infty}$	$Pt$ , psia	$Tt$ , °F
15-in. Mach 6	6.0	0.004	0.5	0.2	1.40	45	780
			4.0	1.7		240	470
20-in. Mach 6	6.0	0.0075	0.5	0.4	1.40	30	400
			1.0	0.8		60	425
			2.0	1.6		125	450
			4.0	3.2		250	475
			7.6	6.1		475	475
31-in. Mach 10	10.0	0.0075	0.5	0.4	1.40	350	1350
			1.1	0.9		720	1350
			2.2	1.8		1450	1350
			7.6	6.1		475	475
20-in. Mach 6 CF <sub>4</sub>	6.0	0.004	0.5	0.2	1.22	1600	800

### Data Acquisition, Reduction, and Uncertainties

Aerodynamic data were obtained using six-component force-and-moment balances for an angle-of-attack range from 20 to 45 deg. The test procedure was essentially the same for all tunnels. Flow was established in the test section; the model was injected and moved through an angle-of-attack range in a pitch-pause manner; then the model was retracted, and the tunnel shut down. Data were recorded and averaged over a 1- or 2-s interval at the selected angles of attack. Data were recorded continuously in the 15-in. Mach 6 and 20-in. CF<sub>4</sub> Tunnels with the model at one angle of attack. These data were then averaged over a user-defined time period. Flow conditions were determined either from calibrations using stagnation values as input conditions or from the ratio of a pitot probe pressure to the stagnation pressure to obtain the Mach number. Difficulties in determining flow conditions at low stagnation pressure ( $Pt \approx 30$  psia,  $Re_{\infty} = 0.5 \times 10^6$ ) in the 20-in. Mach 6 Tunnel are discussed in a paper by Miller.<sup>11</sup> Data at these Reynolds number are only given as increments, and not for the aerodynamic coefficients  $C_N$  and  $C_m$ .

The nominal flow conditions for each of the facilities are listed in Table 2. Several balances were used in order to provide accurate data over the wide range of loads encountered in the facilities. The balances were mounted either on straight stings or on a blade sting arrangement. Except for the helium-tunnel data, the balances were water-cooled to minimize errors due to heating of the balance. Weight tares, sting deflections under load, and balance interactions were accounted for in the usual manner for each tunnel.<sup>12</sup> Base pressure was measured at one or two locations during each run and used to correct the data to freestream pressure on the base. All data are presented about a moment reference center of 65% of the reference body length. Two sting placements were used: a straight sting through the base, and a blade sting that replaced the vertical tail. The effect of sting placement and the effect of model scale were small, and are discussed in greater detail in a paper by Paulson and Brauckmann.<sup>13</sup> The accuracy of the experimental data was determined using the small-sample method presented by Kline and McClintock.<sup>14</sup> The uncertainties associated with balance accuracy ( $\pm 0.5\%$  full load), angle of attack ( $\pm 0.1$  deg), and freestream pitot pressure (see Table 3) are allowed for. Freestream pitot pressure variations, as determined by facility calibrations, directly affect the Mach number and therefore dynamic pressure used in nondimensionalizing the data to coefficient form. The accuracies are presented in Table 3.

### Other Experimental Techniques

An oil flow visualization technique was employed to look at separation patterns on the models. The model was painted with a commercially available high-temperature flat-black paint. Next a thin coat of clear silicon oil of desired viscosity was applied. A mixture

**Table 3 Experimental uncertainties**

Tunnel	Balance	Scale	$Re_{\infty, L}, \Delta P_{T2}$		$C_N$	$C_m$
			$10^6$	%		
15-in. Mach 6	CF4-3B 2039CM	0.004	0.2	2.0	$\pm 0.0251$	$\pm 0.0057$
			1.7	2.0	0.0201	0.0043
20-in. Mach 6	2044A 2030	0.0075	0.9	2.0	$\pm 0.0322$	$\pm 0.0090$
			0.8	1.4	0.0213	0.0045
			1.6	1.1	0.0131	0.0023
			3.2	0.7	0.0136	0.0048
31-in. Mach 10	2044A	0.0075	5.6	0.4	0.0076	0.0026
			0.4	2.0	$\pm 0.0345$	$\pm 0.0076$
			0.8	1.0	0.0208	0.0045
20-in. Mach 6 CF <sub>4</sub>	CF4-3B	0.004	1.7	1.0	0.0147	0.0023
			0.20	2.0	$\pm 0.0233$	$\pm 0.0036$

of oil and white artist's pigment was then applied by flicking the end of a small brush dipped into the oil mixture, so that the model was covered with many small dots of oil. Flow was established in the tunnel, and the model injected at the desired angle of attack. After a brief period, on the order of 5 s, the model was retracted. Photographs were taken outside the tunnel after the run. Schlieren photographs of the flowfield around the model were taken using a double-pass schlieren system in both Mach 6 air tunnels as well as the 20-in. CF<sub>4</sub> tunnel.

**Computational Method**

The LAURA (Langley aerothermodynamic upwind relaxation algorithm) code was used in this study to solve the thin-layer Navier–Stokes equations. A description of this code is presented in detail in several papers by Gnoffo et al.<sup>15–17</sup> The inviscid first-order flux is constructed using Roe's<sup>18</sup> flux-difference-splitting and Harten's<sup>19</sup> entropy fix with second-order corrections based on Yee's<sup>20</sup> symmetric total-variation-diminishing scheme. A seven-species (N, O, N<sub>2</sub>, O<sub>2</sub>, NO, NO<sup>+</sup>, and e<sup>-</sup>) chemical reaction model is used for the nonequilibrium computations. The usual no-slip boundary condition for viscous flow is applied at the wall, and freestream conditions are set at points on the outer boundary of the computational domain. The exit plane is set so that the inviscid outer flow is supersonic. The computations presented allow for a variable wall temperature. These values are based on the radiation equilibrium temperature at the wall, and were determined from computed heating rates. A catalytic wall boundary condition was used, based on Scott's<sup>21</sup> recombination rates for nitrogen and those of Zoby et al.<sup>22</sup> for oxygen. A multiblock solution strategy is applied in two stages. The first stage may be regarded as a space marching solution, like the parabolized Navier–Stokes (PNS) methods, except that three-dimensional data blocks are employed rather than two-dimensional data planes. The second stage is a conventional, global relaxation, which uses the first-stage solution as an initial condition. The computational results presented herein are discussed further, and with more detail about the code and solution procedure, in papers by Weilmuenster et al.<sup>23,24</sup>

**Results and Discussion**

**Ideal-Gas Results at Mach 6 and 10 in Air**

For the low- to midhypersonic Mach numbers the flight-to-preflight discrepancy is small. Postflight analyses of heating data indicate that the orbiter windward-surface boundary layer is everywhere turbulent. Results at Mach 6 are presented showing the effect of Reynolds number on  $C_N$  and  $C_m$  for the baseline (zero control-surface deflections) in Figs. 2a and 2b, respectively. The data show only a slight effect of Reynolds number.  $C_N$  is decreased and  $C_m$  is slightly nose-down with increasing Reynolds number; however, it should be noted that most of this is within the accuracy of the data, especially for the lower Reynolds numbers (and hence dynamic pressures). Results for a body-flap deflection of 16.0 deg are shown in Figs. 2c and 2d.  $C_N$  is approximately the same for all Reynolds numbers, indicating an increase relative to the baseline configuration. The pitching moment shows a marked nose-down increment with increasing Reynolds number, indicating a more effective body-flap as Reynolds number increases. The cause of these

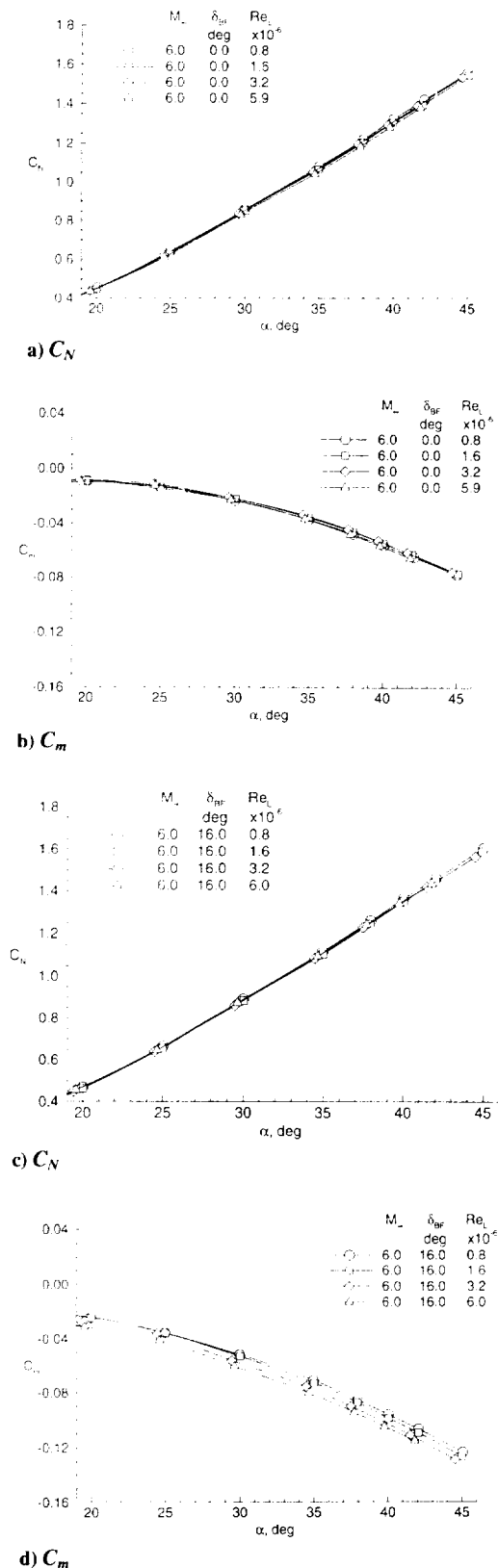


**Fig. 2 Effect of Reynolds number on Shuttle Orbiter aerodynamics.**

effects can be traced to changes in the location of boundary-layer separation and reattachment in front of and on the body flap. Surface streamline patterns (oil flows) on the windward surface in the vicinity of the body flap are shown in Figs. 3a–3d. The model is at an angle of attack of 40 deg with a body-flap deflection of 16.0 deg. As the Reynolds number increases, the separation region shrinks. While the forward separation line moves rearward a small amount, the main effect is the forward motion of the reattachment line on the

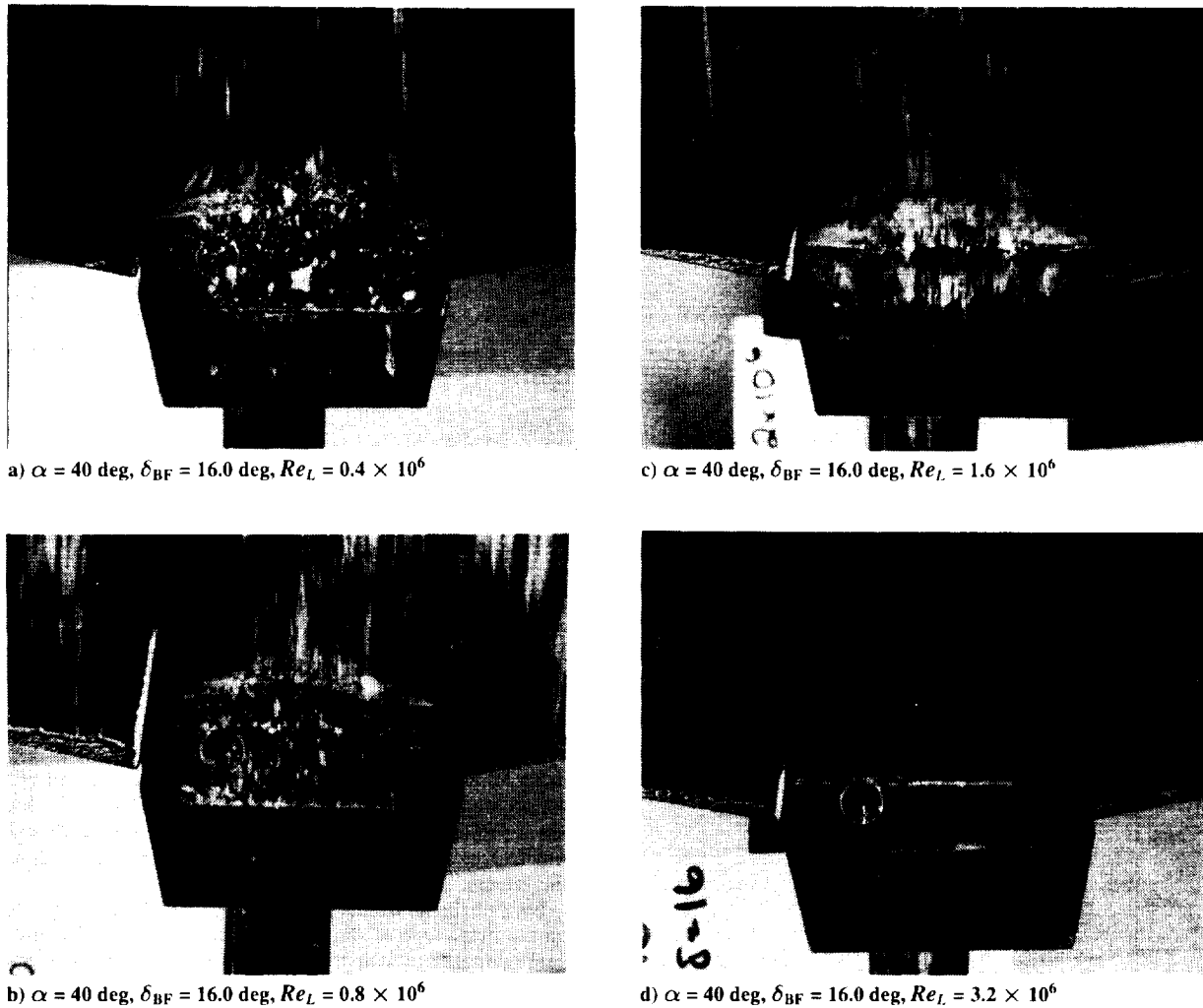


Fig. 3 Oil flow visualization of body-flap region in 20-in. Mach 6 tunnel.

flap itself. The separation is not as well defined at a length Reynolds number of  $1.6 \times 10^6$ ; the oil appeared somewhat smeared or runny. Several repeat runs were made, which verified this pattern. It is postulated that the flow is, or is near, transitional; at the next Reynolds number tested,  $Re_L = 3.2 \times 10^6$ , the flow overcomes the pressure gradient due to the deflected flap and remains attached on the whole lower surface, and the oil flow appears clear and sharp again.

Similar aerodynamic and oil-flow results were observed at Mach 10. The data and oil-flow photographs can be found in papers by Brauckmann et al.<sup>25</sup> and Paulson and Brauckmann.<sup>13</sup> At  $M_\infty = 10$ , no limiting case of flap effectiveness was obtained, as at  $M_\infty = 6$ , presumably because there was insufficient Reynolds-number variation to achieve transitional flow.

Comparisons of the current  $M_\infty = 6$  and  $M_\infty = 10$  results with the preflight prediction (ADDDB) and to STS-1 mission flight-derived data points are made in Figs. 4a–4c. The highest-Reynolds-number experimental data are used, but are still below flight values. All data are interpolated at flight values of  $\alpha$ , referenced to a center-of-gravity location of  $0.65L$ , and the flight-derived data points have been adjusted to zero control-surface deflection using the ADDDB effectiveness values.

The agreement of the current values of  $C_N$  with the data book is very good. Both the current data and the preflight prediction overestimate the the flight  $C_N$  by a slight amount. The agreement in pitching moment is not as good, especially at Mach 10. Values from the ADDDB are in between the current data and flight. The discrepancy between the current data and flight represents a movement in c.p. location of 7.7 in., or 0.6% of the body length. It is probable that nonideal-gas effects are present. Also, recall that the flight data were corrected using ADDDB control-surface effectiveness values.

The body-flap effectiveness  $\Delta C_m$  at  $M_\infty = 6$  and 10 is compared with the preflight prediction in Fig. 4c. The Reynolds number has a small effect on the basic body pitching moment at these Mach numbers, primarily affecting body-flap effectiveness. As just shown, the predicted body-flap effectiveness is bounded by the current tests. Although not duplicating the preflight data book, the current tests are in line with the results. Conventional hypersonic wind tunnels (nonimpulse) are therefore able to accurately describe the aerodynamics of this class of entry vehicles at these low- to midhypersonic Mach numbers. Proper determination of flight control-surface effectiveness requires proper simulation of the state of the boundary layer (laminar, transitional, or turbulent).

#### Computational Predictions

Computational fluid dynamics (CFD) was used to examine differences between ideal-gas and real-gas flowfields. Ideal-gas flowfields can be duplicated in the wind tunnel, whereas in this study real-gas effects were only simulated. Solutions for the modified orbiter geometry corresponding to wind-tunnel and flight conditions were obtained at angles of attack of 35, 40, and 45 deg for body-flap deflections of 0, 5, 10, 15, and 20 deg. The data were interpolated for body-flap deflections of 16.0 and 16.3 deg, to compare with data from the wind-tunnel tests. The input conditions for which solutions were obtained are given in Table 4. A more complete discussion of these results can be found in a paper by Weilmuenster et al.<sup>23</sup> A comparison of the predicted values with wind-tunnel data for the modified orbiter configuration was made, and the results are discussed by Paulson and Brauckmann.<sup>13</sup> The predictions were in good qualitative agreement, although the code overpredicted  $C_N$  by about 2.5%. Differences in  $C_m$  amounted to 1% error in c.p. location.

Table 4 Computational points

Case	Flight	Altitude, km	GMT, s	$\alpha$ , deg	$\delta_{BF}$ , deg	$\delta_c$ , deg	$M_\infty$
1	STS-1	73.1	64748	39.4	15.973	-0.444	23.68
2	STS-2	72.4	75620	39.4	14.914	1.7436	24.3
3	STS-2	64.4	75950	41.2	13.54	1.511	18.07
4	STS-2	54.8	76130	39.7	12.92	0.74	12.85
5	Wind tunnel	—	—	40.0	—	—	10.00

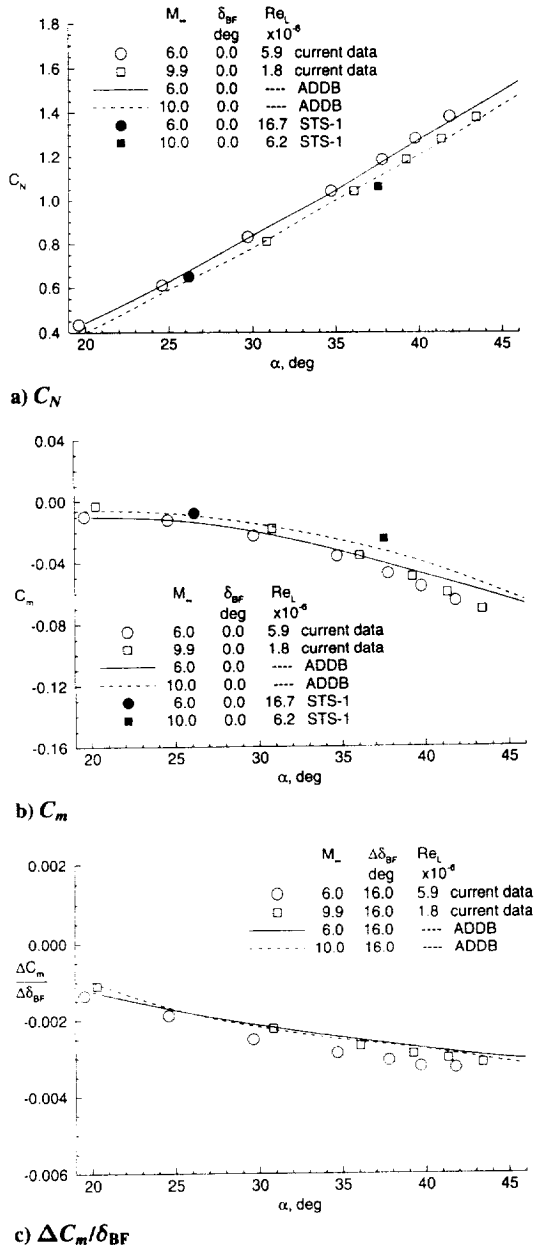


Fig. 4 Comparison of present results with ADDB and flight (STS-1).

In order to examine the differences in the flowfield that occur in flight, computations were carried out using finite-rate chemistry on the modified orbiter geometry at flight conditions. As shown in Fig. 5, the occurrence of high temperatures associated with this flight condition dissociates the flow within the shock layer so that the ratio of specific heats,  $\gamma$ , defined here as  $h/e$ , is reduced from 1.4 in the freestream, to 1.3 immediately behind the shock, to about 1.14 near the body. In the nose region,  $\gamma$  is reduced to about 1.12. The major effect of this change in  $\gamma$  is a lowering of the surface pressure on the last 20% of the vehicle. A plot of the computed centerline surface pressure for wind-tunnel and flight conditions is given in Fig. 6. Included are results from a solution at a Mach number of 24

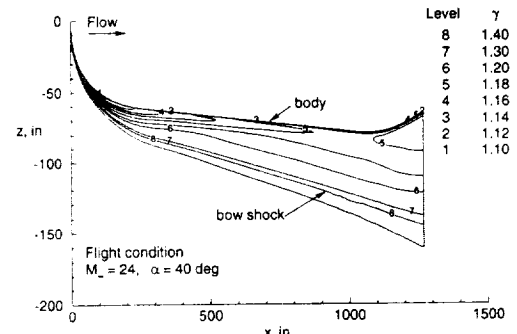
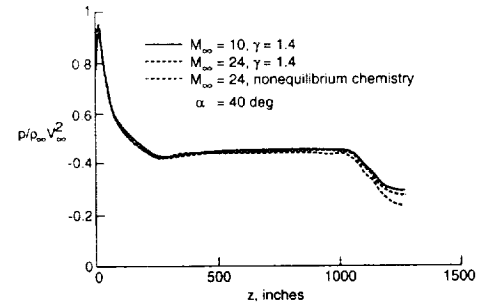
Fig. 5 Computed variation of  $\gamma$  in windward flowfield of modified Orbiter.

Fig. 6 Computed centerline surface pressure for modified Orbiter.

using an ideal-gas value for  $\gamma$  of 1.4. There is a small difference due to Mach number itself, but the largest difference is due to the lower  $\gamma$ . The lower  $\gamma$  results in the expansion on the aft end occurring to a greater degree, lowering the pressure over a large area of the vehicle.

It should be noted that the Orbiter geometry has a large influence on the magnitude of the real-gas effects. The Orbiter has an expansion that starts at approximately  $0.8L$ , which coincides with the largest planform area, and thus the expansion of the flow, relative to ideal-gas flow, lowers the pressure over a large area. The effect of this reduced pressure on the aerodynamic coefficients is shown in Figs. 7a and 7b. The lower pressure on the aft end causes a reduction in normal force and a nose up pitching-moment increment. The computed increment in  $C_N$  between tunnel and flight conditions is 0.062 and 0.048 for  $\delta_{BF} = 0.0$  and 16.3 deg, respectively. This agrees well with the increment found in flight,  $\Delta C_N = 0.059$  (preflight ADDB to flight, STS-1). The increment in  $C_m$  for  $\delta_{BF} = 0.0$  deg is 0.040, which is larger than the increment found between flight and preflight prediction. For the 16.3-deg flap case, however, the increment is 0.028, which is very close to that found between the preflight ADDB and flight. The difference in the two increments can be traced to greater flap effectiveness at flight conditions.

There are two reasons for the greater calculated flap effectiveness. The predicted separation region in front of and on the flap is smaller in flight than in the wind tunnel for the same length Reynolds number. Calculated streamline patterns in the region of the body flap at both tunnel and flight conditions for a flap deflection of 20 deg are shown in Figs. 8a and 8b. The much smaller separation region for flight conditions is evident. In addition, as discussed by Weilmuenster et al.,<sup>23</sup> the pressure rise on the flap was higher in flight than in the wind tunnel, but this was due to a combination of Mach and  $\gamma$  effects. In fact, the lower  $\gamma$  tends to reduce the pressure rise, but the higher Mach number in the shock layer in flight overcomes this. A solution at  $M_\infty = 24$  (flight) but with  $\gamma = 1.4$  (ideal gas) was not obtained on the deflected flap configuration; thus a separation of these effects cannot be made.

An analysis of control-surface effectiveness was performed after the first few flights of the Shuttle Orbiter.<sup>8</sup> Both an elevon and a body-flap pulse maneuver were analyzed in terms of c.p. location for predicted and flight performance. While the results were biased from the perfect correlation line, the conclusion was reached that flap effectiveness, as presented in the preflight ADDB, was predicted correctly. More analysis of this discrepancy is needed.

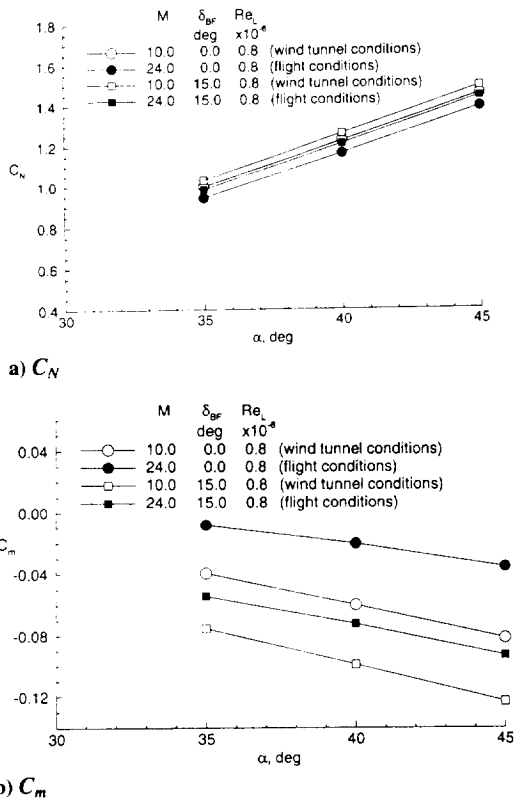


Fig. 7 Comparison of modified Orbiter aerodynamics at wind tunnel and flight conditions.

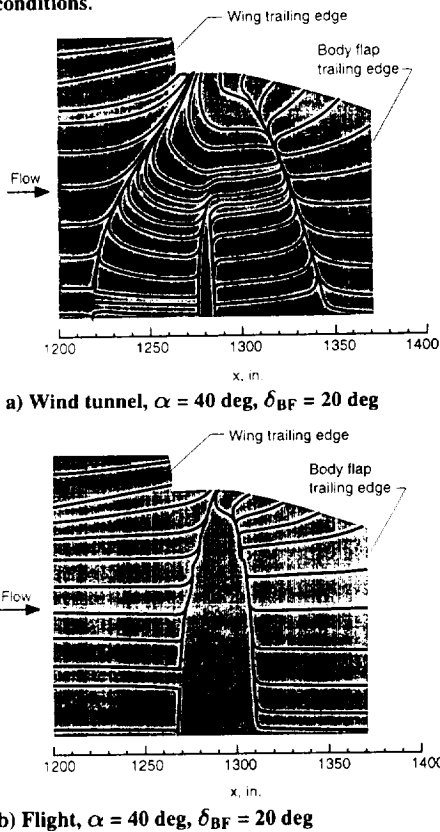


Fig. 8 Calculated surface streamline patterns in vicinity of body flap at wind-tunnel and flight conditions.

High-Mach-Number Simulation

Two facilities at Langley were used to examine the high-Mach-number flight regime: the 22-in. Mach 20 Helium tunnel and the 20-in. Mach 6  $CF_4$  tunnel. The helium tunnel uses purified helium, which behaves as an ideal gas with a  $\gamma$  of 1.667. There are a number of advantages to testing with helium, the primary one being that very high values of  $Re_L$  may be generated at high Mach numbers without

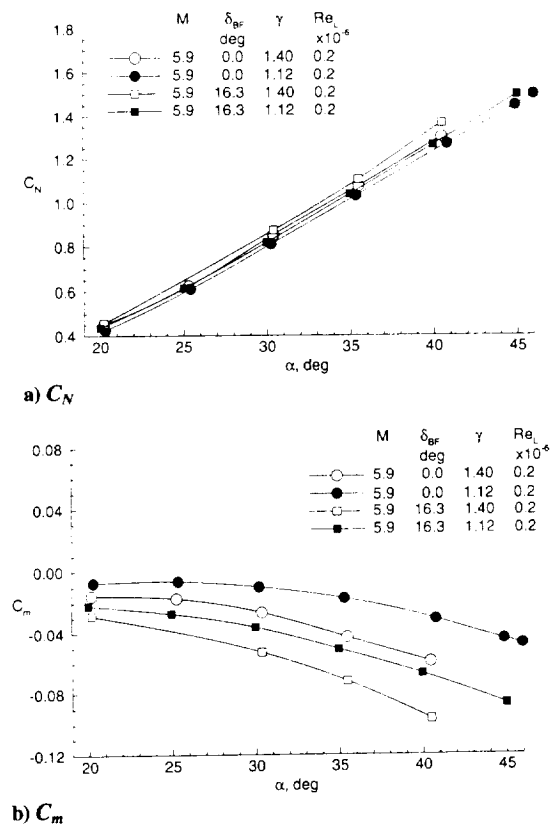


Fig. 9 Comparison of Shuttle Orbiter aerodynamics in air and  $CF_4$ .

having to heat the gas to prevent liquefaction. For this study, the facility provided a close match of flight Mach and Reynolds numbers. However, the flowfield  $\gamma$  remained at  $\gamma = 1.667$ . The results from the helium-tunnel tests<sup>25</sup> showed a significant nose-down pitching moment compared to flight, which can be explained by  $\gamma$  being higher rather than lower than ideal air. In addition, the body-flap effectiveness was reduced. Thus, testing in helium is inappropriate for the simulation of real-gas effects.

The  $CF_4$  tunnel uses a heavy gas that has a  $\gamma$  lower than ideal air to simulate this aspect of real-gas flows such as occurs in flight.<sup>26,27</sup> The value of  $\gamma$  in the  $CF_4$  tunnel, around 1.15 in the shock layer, is close to that determined to occur in flight. A comparison of aerodynamic coefficients obtained in air and  $CF_4$  at identical values of Reynolds number and Mach number is given in Figs. 9a and 9b. As can be seen, testing in a heavy gas decreases the normal-force coefficient and causes a nose-up pitch increment, when compared with results in air. The decrease in  $C_N$  is 0.046 for  $\delta_{BF} = 0.0$  deg and 0.077 for  $\delta_{BF} = 16.3$  deg. This decrement is approximately the same as the flight decrement and that determined by the CFD analysis. The change in  $C_m$  is 0.029 for  $\delta_{BF} = 0.0$  deg and 0.027 for  $\delta_{BF} = 16.3$  deg. This increment is the same as the flight-to-preflight increment, but unlike the CFD solutions, the increment is the same for the undeflected and deflected body-flap configurations. For this configuration, then, with an expansion region on the windward surface, the real-gas effects are closely approximated by testing in a heavy gas such as  $CF_4$ .

Conclusions

A study was undertaken at the Langley Research Center to resolve the cause of the pitch-up anomaly observed during entry of the first flight of the Shuttle Orbiter. Tests in five hypersonic wind tunnels were conducted using Shuttle Orbiter and modified Orbiter (windward surface accurately modeled, leeside surface modeled by elliptical cross sections) configurations to examine the effects of Mach number, Reynolds number, and ratio of specific heats. In addition, computational solutions for wind-tunnel and flight conditions were obtained to complement the experimental results, and to extend the analysis to flight conditions.

The low-hypersonic, ideal-gas wind tunnels adequately predicted flight aerodynamics when no real-gas effects were present. Varying

the freestream Mach number from 6 to 10 decreased  $C_N$  slightly, with a small nose-up increment to the pitching moment. Varying the Reynolds number did not significantly affect the basic body (zero control-surface deflections) pitching moment, but did affect body-flap effectiveness, by altering the location of flow separation and reattachment on the control surface. A limiting case for control effectiveness may have been obtained (at  $M_\infty = 6$ ) when the boundary-layer flow approaching the control surface became fully turbulent and the flow stayed completely attached.

At high-Mach-number flight conditions, a marked decrease in the specific heat ratio  $\gamma$  of the gas in the shock layer occurs because of high-temperature effects. The primary effect of this lower specific heat ratio within the flowfield of the Orbiter is lower pressures on the aft windward expansion surface of the Orbiter, relative to those deduced from hypersonic wind-tunnel tests with ideal- or near-ideal-gas test flows, and thus a corresponding nose-up pitching moment. Computationally, good agreement with the flight aerodynamic coefficients was obtained with the flap deflected to approximately 16 deg. Testing in a heavy gas in the 20-in. Mach 6 CF<sub>4</sub> tunnel gave a good simulation of high temperature effects, as the aerodynamic increments and flap effectiveness were in good agreement with flight results.

The overall agreement between flight, computational solutions at flight conditions (laminar boundary layer, continuum flow regime), and measurements made in the CF<sub>4</sub> tunnel was quite good. This study has demonstrated that a preferred approach to accurately determine the hypersonic aerodynamic characteristics of future winged or lifting-body space transportation system concepts is to test high-fidelity models in conventional facilities to provide baseline and parametric data for hypersonic design optimization. High-temperature effects should be simulated by testing in a heavy-gas facility. Complementary CFD solutions should also be obtained to substantiate these results and provide information at flight conditions, thus giving high confidence in the predicted aerodynamics.

### References

- <sup>1</sup>Griffith, B. J., Maus, J. R., and Majors, B. M., "Addressing the Hypersonic Simulation Problem," AIAA Paper 86-9775, April 1986.
- <sup>2</sup>Compton, H. R., Schiess, J. R., Suit, W. T., Scallion, W. I., and Hudgins, J. W., "Stability and Control over the Supersonic and Hypersonic Speed Range," NASA CP-2283, Pt. 1, Oct. 1983, pp. 309-346.
- <sup>3</sup>Griffith, B. J., Maus, J. R., and Best, J. T., "Explanation of the Hypersonic Longitudinal Stability Problem—Lessons Learned," NASA CP-2283, Pt. 1, March 1983, pp. 347-380.
- <sup>4</sup>Calloway, R. L., "Real Gas Simulation for the Shuttle Orbiter and Planetary Entry Configurations Including Flight Results," AIAA Paper 84-0489, Jan. 1984.
- <sup>5</sup>Anderson, J. D., "High-Temperature Gas Dynamics: Some Introductory Considerations," *Hypersonic and High Temperature Gas Dynamics*, McGraw-Hill, 1989, pp. 363-376.
- <sup>6</sup>Koppenwallner, G., "Low Reynolds Number Influence on Aerodynamic Performance of Hypersonic Lifting Vehicles," *Aerodynamics of Hypersonic Lifting Vehicles*, AGARD-CP-428, April 1987.
- <sup>7</sup>Anon., "Aerodynamic Design Data Book—Orbiter Vehicle," Rockwell International, Space Division, SD72-SH-0060-1M, Vol. 1, Nov. 1980.

- <sup>8</sup>Romere, P. O., and Whitnah, A. M., "Space Shuttle Entry Longitudinal Aerodynamic Comparison of Flights 1-4 with Preflight Predictions," NASA CP-2283, Pt. 1, March 1983, pp. 283-307.
- <sup>9</sup>Woods, W. C., Arrington, J. P., and Hamilton, H. H., II, "A Review of Preflight Estimates of Real Gas Effects on Space Shuttle Aerodynamic Characteristics," NASA CP-2283, Pt. 1, Oct. 1983, pp. 309-346.
- <sup>10</sup>Miller, C. G., "Langley Hypersonic Aerodynamic/Aerothermodynamic Testing Capabilities—Present and Future," AIAA Paper 90-1376, June 1990.
- <sup>11</sup>Miller, C. G., and Smith, F. M., "Langley Hypersonic Facilities Complex—Description and Application," AIAA Paper 86-0741, March 1986.
- <sup>12</sup>Keyes, J. W., "Force Testing Manual for the Langley 20-in. Mach 6 Tunnel," NASA TM-74026, July 1977.
- <sup>13</sup>Paulson, J. W., Jr., and Brauckmann, G. J., "Recent Ground-Facility Simulations of Shuttle Orbiter Aerodynamics," *Orbiter Experiments (OEX) Aerothermodynamics Symposium*, NASA CP-3248, Nov. 1994.
- <sup>14</sup>Kline, S. J., and McClintock, F. A., "Describing Uncertainties in Simple-Sample Experiments," *Mechanical Engineering*, Jan. 1953, pp. 3-8.
- <sup>15</sup>Gnoffo, P. A., Gupta, R. N., and Shinn, J., "Conservation Equations and Physical Models for Hypersonic Air Flows in Thermal and Chemical Nonequilibrium," NASA TP-2867, Feb. 1989.
- <sup>16</sup>Gnoffo, P. A., "Upwind-Biased, Point-Implicit Relaxation Strategies for Viscous Hypersonic Flows," AIAA Paper 89-1972, June 1989.
- <sup>17</sup>Gnoffo, P. A., "An Upwind Point Implicit Relaxation Algorithm for Viscous Compressible Perfect-Gas Flows," NASA TP-2953, Feb. 1990.
- <sup>18</sup>Roe, P. L., "Approximate Riemann Solvers, Parameter Vectors, and Difference Schemes," *Journal of Computational Physics*, Vol. 43, 1981, pp. 357-372.
- <sup>19</sup>Harten, A., "High Resolution Schemes for Hyperbolic Conservation Laws," *Journal of Computational Physics*, Vol. 49, 1983, pp. 357-393.
- <sup>20</sup>Yee, H. C., "On Symmetric and Upwind TVD Schemes," NASA TM-86842, Sept. 1985.
- <sup>21</sup>Scott, C. D., "Catalytic Recombination of Oxygen and Nitrogen in High-Temperature Surface Insulation," *Aerothermodynamics and Planetary Entry*, edited by A. L. Crosbie, Vol. 77, Progress in Astronautics and Aeronautics, AIAA, New York, 1981, pp. 192-212.
- <sup>22</sup>Zoby, E. V., Gupta, R. N., and Simmons, A. L., "Temperature Dependent Reaction Rate Expressions for Oxygen Recombination," *Thermal Design of Aeroassisted Orbital Transfer Vehicles*, edited by H. F. Nelson, Vol. 96, Progress in Astronautics and Aeronautics, AIAA, New York, 1985, pp. 445-465.
- <sup>23</sup>Weilmuenster, K. J., Gnoffo, P. A., and Greene, F. A., "Navier-Stokes Simulations of Orbiter Aerodynamic Characteristics Including Pitch Trim and Body Flap," *Journal of Spacecraft and Rockets*, Vol. 31, No. 3, 1994, pp. 355-366; AIAA Paper 93-2814, July 1993.
- <sup>24</sup>Weilmuenster, K. J., and Gnoffo, P. A., "Solution Strategy for Three-Dimensional Configurations at Hypersonic Speeds," *Journal of Spacecraft and Rockets*, Vol. 30, No. 4, 1993, pp. 385-394.
- <sup>25</sup>Brauckmann, G. J., Paulson, J. W., and Weilmuenster, K. J., "Experimental and Computational Analysis of the Space Shuttle Orbiter Hypersonic 'Pitch-Up Anomaly,'" AIAA Paper 94-0632, Jan. 1994.
- <sup>26</sup>Jones, R. A., and Hunt, J. L., "Use of Tetrafluoromethane to Simulate Real-Gas Effects on the Hypersonic Aerodynamics of Blunt Vehicles," NASA TR T-312, June 1969.
- <sup>27</sup>Midden, R. E., and Miller, C. G., "Description and Calibration of the Langley Hypersonic CF<sub>4</sub> Tunnel," NASA TP-2384, March 1985.

J. C. Adams  
Associate Editor